JOURNAL OF GEOPHYSICAL RESEARCH, VOL. 106, NO. D12, PAGES 12,477–12,488, JUNE 27, 2001

Algorithm development strategies for retrieving the downwelling longwave flux at the Earth's surface

Yaping Zhou

Analysis Branch, Climate Prediction Center, National Centers for Environmental Prediction, National Weather Service, National Oceanic and Atmospheric Administration, Washington, D. C.

Robert D. Cess

Marine Sciences Research Center, State University of New York at Stony Brook, Stony Brook, New York

Abstract. Algorithm development strategies for retrieving the surface downwelling longwave flux (SDLW) have been formulated on the basis of detailed studies with radiative transfer models and observational data. The model sensitivity studies were conducted with the column radiation model from the National Center for Atmospheric Research Community Climate Model Version 3 and the Moderate-Resolution Transmittance radiation model. The studies show the clear-sky SDLW can be largely determined from only two parameters: the surface upwelling longwave flux and the column precipitable water vapor. Cloudy-sky sensitivity tests show that, as would be expected, cloud base height is an important factor in determining the SDLW, especially for low clouds. However, when considering broken clouds as occur in reality, there is no way of logically defining an average cloud base height. Instead, cloud liquid water path is shown to be a preferable parameter for use in an all-sky algorithm, not because it serves as a direct cloud input parameter, but rather that it serves as a useful surrogate for cloud base height. Observational data from the Atmospheric Radiation Measurements Program at the U.S. Southern Great Plains (SGP) Oklahoma Central Facility and the Tropical Western Pacific (TWP) Manus Island were used in deriving and validating an illustrative algorithm. The observations show similar relations as found in the model sensitivity tests and suggest that a single algorithm could be applicable for both clear and cloudy conditions as well as for diverse geographical locations. For example, when applied to the TWP data, an algorithm based on a regression of SGP all-sky data produces a relative bias error in SDLW of only 1.4% under all-sky conditions and −0.2% for clear skies.

1. Introduction

The surface radiation budget not only represents direct radiative forcing at the surface, but it also determines the latent and sensible heating fluxes to the atmosphere. The surface net longwave (LW) flux is further a manifestation of the greenhouse effect of the atmosphere, and it is essential to reproduce it accurately. Direct surface radiation measurements, however, are geographically sparse. Over the years many algorithms have been developed in an effort to obtain a global surface radiation data set. The upward emission from the surface (SULW) is usually determined from the Stephen-Boltzmann law given knowledge of the surface temperature and, if available, the surface emissivity. The surface downwelling longwave flux (SDLW) is the most difficult component, since it is significantly affected by the vertical distribution of clouds.

Bulk formulas have been used extensively in the past for estimating SDLW for large-scale studies. These formulas rely on surface or near-surface meteorological variables, such as surface temperature and humidity, and in some cases an estimated cloud amount [*Berliand and Berliand*, 1952; *Idso and Jackson*, 1969; *Brutsaert*, 1975; *Idso*, 1981; *Swinbank*, 1963; *Satterlund*, 1979; *Prata*, 1996]. *Fung et al*. [1984] conducted a detailed examination of several widely used bulk formulas, using computations from a detailed radiative transfer model, and found large discrepancies. They pointed out that cloud base height, optical thickness, and cloud type have strong impacts on the surface net longwave flux and concluded that it was not possible to use a single cloudiness factor in a bulk formula to evaluate the instantaneous SDLW for overcast skies.

Several techniques have been developed for deriving the SDLW from satellite measurements. *Smith and Woolf* [1983] demonstrated a regression technique, where upward, downward, and net LW fluxes at various levels in the atmosphere were computed from outgoing radiances measured by several Visible and Infrared Spin Scan Radiometer Atmospheric Sounder channels. *Schmetz et al*. [1986] used the bulk formulas of *Idso and Jackson* [1969] and *Idso* [1981] to determine the SDLW, using surface temperature fields from grid point analyses and cloud parameters derived from Meteosat data. *Frouin et al*. [1988] presented a radiative transfer methodology for estimating the downward longwave radiation over oceans using TIROS Operational Vertical Sounder meteorology together with cloud parameters derived from GOES data. *Gupta* [1989] and *Gupta et al*. [1992] have developed an algorithm to derive the surface longwave fluxes from NOAA operational sun-synchronous satellite data. This algorithm is used to produce the gridded monthly surface longwave fluxes as part of the

Paper number 2001JD900144.
0148-0227/01/2001JD900144$09.00

Surface Radiation Budget project by using the International Satellite Cloud Climatology Project-C1 data as its primary input data.

There have also been some attempts to obtain the surface longwave fluxes by exploring the relationships between the top of the atmosphere (TOA) and surface fluxes. For clear skies, *Inamdar and Ramanathan* [1997] developed an algorithm that expresses a normalized surface longwave flux and TOA flux in terms of column water vapor amount and TOA radiative measurements in the LW window (8 to 11 μm). *Stephens et al*. [1994] have utilized the outgoing LW radiation (OLR) to derive the monthly mean SDLW on the basis of a linear regression of SDLW/OLR with column water vapor. Their results are restricted to clear skies and ice-free ocean areas. *Harshvardhan et al*. [1990] used simulations from a general circulation model (GCM) to estimate a climatological ratio of cloud longwave forcing (CLF) at the TOA and at the surface along with the CLF obtained from Earth Radiation Budget Experiment data to obtain the surface CLF. The surface downwelling and net longwave fluxes for cloudy skies were obtained by adding the surface CLF to the clear-sky fluxes, which were calculated from soundings using a radiation model. While this technique avoids the input of cloud information, it is subject to uncertainty because of the GCM-based CLF ratios.

As there is no simple relation between the surface longwave flux and the TOA flux [*Ramanathan*, 1986], especially for cloudy skies, satellite retrievals normally rely on retrieved atmospheric temperature, water vapor, and ozone profiles, along with cloud properties, by applying them to radiation models and/or algorithms. The disadvantage of such techniques is that they are highly dependent on the satellite-retrieved atmospheric profiles and cloud parameters that are subject to large uncertainties.

Without accurate measurements of cloud amount and base temperature, estimates of the cloudy-sky SDLW remain a challenge. In this paper we present strategies for developing an algorithm to retrieve the SDLW on the basis of physical models as well as observational data for all-sky conditions. A suggested new algorithm requires input of surface temperature, total precipitable water vapor (PWV) and cloud liquid water path (LWP). The advantage of this technique is that the only cloud parameter required is cloud liquid water which can be measured by both surface and satellite microwave instruments. In section 2 we will first conduct model sensitivity tests to see how atmospheric profiles and clouds affect the SDLW. In section 3 we use observational data to verify the results from the model study and to derive an algorithm from the data. In Section 4 we summarize the present work and discuss future improvements.

2. Model Sensitivity Studies

2.1. Radiation Models

Two widely used radiation models are employed in this work: the column radiation model (CRM) that is the standalone version of the LW radiation code used in Version 3 of the National Center for Atmospheric Research Community Climate Model (CCM3). The second is Version 3.7 of the Moderate-Resolution Transmittance (MODTRAN) radiation model. The two models vary in their sophistication and general applications. The CRM is composed of the actual subroutines from CCM3, modified as little as possible in order to run in a standalone mode (available at http://www.cgd.ucar.edu/cms/crm), and the model is based on the absorptivity/emissivity formulation of *Ramanathan and Downey* [1986]. Major absorbers include H_2O, CO_2, and O_3 in addition to the following trace gases: CH_4, N_2O, CFC_{11}, and CFC_{12}. Cloud emissivity is accounted for by an effective cloud amount, which is a function of liquid and ice water content at each model layer [*Kiehl et al*., 1996].

MODTRAN 3.7 is a band model which calculates atmospheric radiance and transmittance for frequencies from 0 to 50,000 cm^{-1} at a nominal spectral resolution of 2 cm^{-1} [*Kneizys et al*., 1988]. It was developed from the Low-Resolution Transmittance (LOWTRAN) code [*Kneizys et al*., 1988]. This band model uses three temperature-dependent parameters, an absorption coefficient, a line density parameter, and an average line width. The spectral region is partitioned into 1 cm^{-1} bins for each molecule, and the absorption within the bin is integrated over a Voigt line shape. The Curtis-Godson approximation is used for multilayer atmospheric calculations. Other important elements include internal aerosols, cloud models, and default atmospheric profiles [*Abreu and Anderson*, 1996]. Model parameters are derived directly from the HITRAN 1992 database [*Rothman et al*., 1992]. The version used in this study, MODTRAN 3.7, has a major upgrade so that users can easily define cloud descriptions. For example, clouds can be placed anywhere within the defined atmosphere, can coexist with aerosols, and can have a mixed phase composition [*Acharya et al*., 1998].

2.2. Clear-Sky Sensitivity Tests Using CRM

The inputs to the CRM are based on the six default MODTRAN atmospheres: tropical, midlatitude summer, midlatitude winter, subarctic summer, subarctic winter, and standard U.S. atmospheres. Three kinds of perturbations are applied to these profiles in order to examine different aspects of the physics.

2.2.1. Total water vapor amount and distribution. Water vapor represents the major greenhouse gas in the atmosphere, and it has the most prominent variation on short timescales. The total precipitable water vapor (PWV) and its vertical distribution are thus critical to the TOA and surface longwave fluxes, and we first fix the vertical temperature profile and prescribe the vertical humidity profile using the formula from *Stephens et al*. [1994]:

$$q = q_s(p/p_s)^{\lambda},$$

where q and p are the water vapor mixing ratio and pressure, respectively, while the subscript s denotes the surface quantities. We employed a set of experiments with $\lambda = 1, 2, 3, 4, 5$ (a value of $\lambda = 3$ is typical of moisture profiles in the Earth's atmosphere) and surface relative humidity ranging from 0.2 to 1.0 with increments of 0.1. Since λ defines the vertical distribution of water vapor, while surface relative humidity controls PWV, these experiments cover most atmospheric water vapor conditions.

2.2.2. Surface temperature and lapse rate. With a fixed mixing ratio the vertical distribution of the longwave flux is determined by the temperature structure of the atmosphere. Two kinds of perturbations were added to the temperature profiles. First, the surface temperature (T_s) was perturbed (from -6 K to $+6$ K with 2 K increments) with fixed lapse rate (Γ) so that the temperature of the whole troposphere is uniformly changed. Second, the lapse rate was modified (from

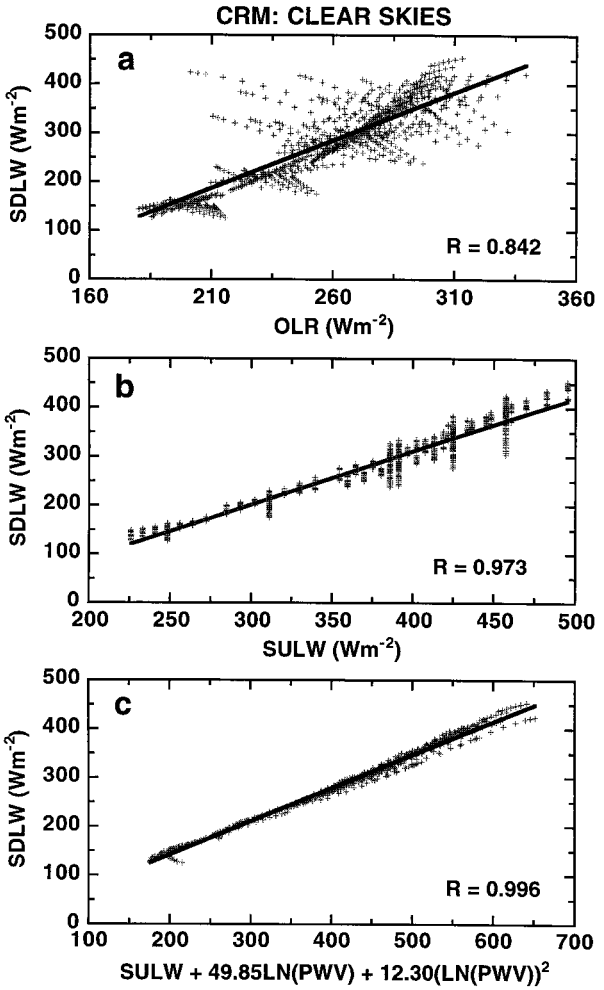

Figure 1. (a) Scatterplot of SDLW versus OLR for CRM and for clear skies. The line denotes a linear fit, and R is the correlation coefficient. (b) Same as Figure 1a, but versus SULW. (c) Same as Figure 1a, but versus a function whose coefficients were determined from a multivariable regression. On figure, "LN" is the natural logarithm.

-1.5 K km^{-1} to 1.5 K km^{-1} with 0.5 K km^{-1} increments) with fixed surface temperature so that the vertical temperature structure was changed. A combination of 49 variations was employed for each of the six default atmospheres. For all the cases, the stratospheric temperature is held fixed. Since the mixing ratio was held fixed, relative humidity changed but not the atmospheric opacity. So any changes in the surface and TOA fluxes are due solely to the change of temperature structure.

2.2.3. Fixed relative humidity. For climate studies a more realistic assumption for the atmosphere is to fix the relative humidity so that a warmer atmosphere contains more moisture than a colder atmosphere [*Manabe and Wetherald*, 1967]. Thus, for the temperature perturbations described in section 2.2.2 we additionally fixed the atmospheric relative humidity so that the mixing ratio changed accordingly.

2.2.4. Results. The clear-sky model sensitivity studies described in sections 2.2.1–2.2.3 provided 888 CRM simulations, and these are summarized in Figure 1, where R denotes the single-variable (Figures 1a and 1b) or multivariable (Figure 1c) correlation coefficient. We have systematically investigated the dependence of SDLW upon SULW, OLR, Γ, and λ. Figure 1 provides the salient results of those studies, where PWV denotes the column precipitable water vapor in centimeters. That SDLW is more strongly correlated with SULW than with OLR (Figure 1b versus Figure 1a) is because SDLW mainly originates from the lower portion of the atmosphere. The multivariable regression of SDLW with SULW and ln (PWV), as shown in Figure 1c, gives the strongest correlation (R = 0.996) that we have found.

For the real atmosphere the temperature-humidity relation is more complicated than used in the present sensitivity study. For short timescales the mixing ratio is usually more stable than is relative humidity, since the latter is sensitive to temperature perturbations through the dependence of the saturation vapor pressure upon temperature. For long timescales, however, relative humidity is considered more stable, but it also depends on different climate regimes. For example, over the tropical oceans the relative humidity in convective regions is higher than in nonconvective regions, which is not only because of the temperature dependence of the saturation vapor pressure but also because of the moistening effect of low-level convergence of moisture, upward transport by deep convection, and the detraining of ice from the associated cirrus anvils [*Sun and Oort*, 1995; *Inamdar and Ramanathan*, 1994]. Nevertheless, the above sensitivity studies provide useful insights as to the dependence of SDLW upon other atmospheric parameters.

2.3. Cloudy-Sky Sensitivity Tests

A cloud is defined by the cloud profile (cloud base, top, thickness), microphysics (cloud droplet size distribution, particle shape, water and ice content, etc.) and radiative properties (spectral extinction, absorption, asymmetry coefficients of water droplets and ice particles, etc.). The CRM has a limited capability for varying the cloud base, top height, and the cloud LWP, but the cloud radiative properties of CRM are fixed. MODTRAN, on the other hand, has several default cloud models and offers more flexibility in user input cloud parameters, so it is used in addition to CRM to study the effects of cloud optical properties on the longwave fluxes.

2.3.1. Cloudy-sky sensitivity tests with MODTRAN. It will be convenient to employ MODTRAN first to demonstrate cloud sensitivity tests. These tests are based on MODTRAN's five model default clouds as summarized in Table 1, and the sensitivity tests consisted of increasing cloud heights by 5 km with 1 km steps and changing the cloud thickness through multiplying the default cloud thickness by 0.5 to 2.5 at 0.5 intervals. This resulted in a total of 750 cases (five cloud base heights, five cloud thicknesses, five cloud types, and six default atmospheres). We chose the relative humidity to be 100% within the cloud layers. In MODTRAN the cloud liquid water density is determined by the cloud type. Since the model cloud water density does not depend on cloud height, the cloud LWP is only a function of cloud thickness for a given type of cloud. As will be emphasized in section 2.3.2, this differs from the CCM3 parameterization for which LWP depends on cloud height.

Figure 2 summarizes the results for overcast clouds (unit cloud fraction) and explores two extensions of the clear-sky correlation of Figure 1c, for which the same type of correlation has been employed in Figure 2a for the overcast clouds. These consist of using either cloud base height (Figure 2b) or LWP (Figure 2c) as a new predictive parameter. Cloud base height

Table 1. Properties of the MODTRAN Cumulus- and Stratus-Type Model Clouds

Cloud Case	Cloud Type	Thickness, km	Base Height, km	0.55 μm Extinction, km^{-1}	Column Liquid, km g^{-1} m^{-3}
1	cumulus	2.34	0.66	92.6	1.664
2	altostratus	0.60	2.40	128.1	0.3450
3	stratus	0.67	0.33	56.9	0.2010
4	stratus/stratocumulus	1.34	0.66	38.7	0.2165
5	nimbostratus	0.50	0.16	92.0	0.3460

(BH) significantly improves the multicorrelation coefficient, increasing it from $R = 0.981$ (Figure 2a) to $R = 0.998$ (Figure 2b), and it clearly is a meaningful cloud input parameter since it governs the emission temperature of the cloud bottom. No such improvement, however, occurs when LWP is used as an input parameter, as is demonstrated in Figure 2c, and this is physically understandable. For clouds that impact SDLW (low level and midlevel) the emissivity of the cloud bottom is essentially unity and thus invariant to LWP. Hence, as Figure 2 demonstrates, one would not anticipate that LWP would constitute a meaningful input parameter.

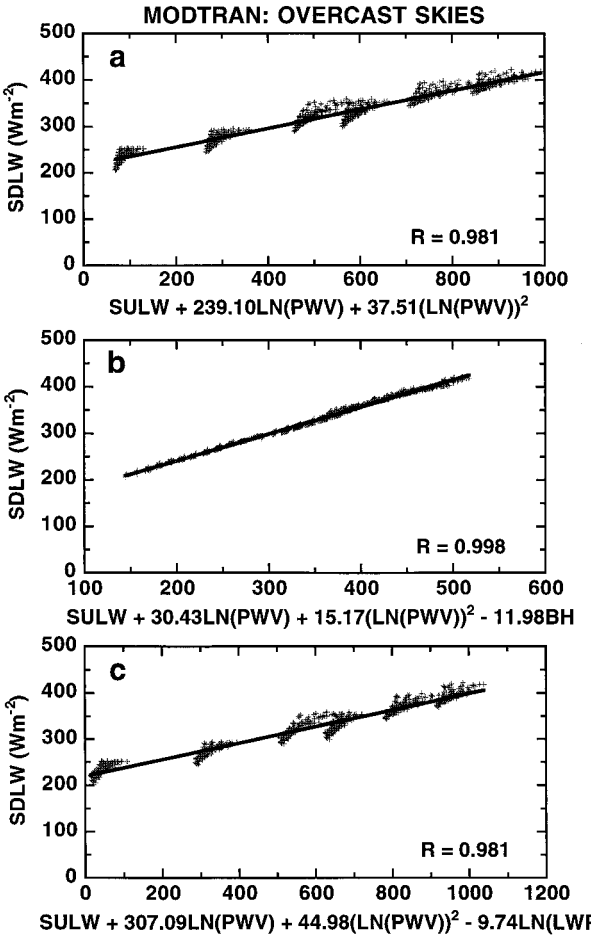

Figure 2. (a) Same as Figure 1c, but for MODTRAN and for overcast skies. (b) Same as Figure 2a, but with cloud base height (BH) included in the x axis variable. (c) Same as Figure 2a, but with cloud liquid water path (LWP) included in the x axis variable.

2.3.2. Cloudy-sky sensitivity tests with CRM. Clouds with various thicknesses and heights were incorporated into CRM, and the six default atmospheres were again utilized. The prescribed cloud thickness ranged from ~0.2 to 7 km, and base heights ranged from 0.3 to 8 km. The relative humidity inside the cloud was again set to 100%. In CCM3, from which CRM was derived, the cloud liquid water density, ρ_1, for each cloud layer depends on altitude [*Kiehl*, 1991] as

$$\rho_1 = \rho_{01} \exp(-z/h_1)$$
$$\rho_{01} = 0.18 \text{ g m}^{-3}, \quad (1)$$

where h_1 is the cloud-water scale height in meters [*Kiehl et al.*, 1996] given by

$$h_1 = 700 \ln[1 + (1/g)\int qdp].$$

In our sensitivity tests, we first compute LWP on the basis of the CCM3 parameterizations given above and then modify the default LWP by multiplying it by a factor of 0.5, 1.0, or 2.0. Cloud fraction was either set to unity (overcast) or to a random amount for each cloud layer, and a total of 1150 simulations was performed for both overcast and random clouds. Although our sensitivity studies are restricted to water clouds, this does not preclude the occurrence of cirrus clouds that, because of their altitude, have virtually no impact upon SDLW.

Figure 3 summarizes the CRM results for overcast clouds (unit cloud fraction) in the same manner as in Figure 2 for MODTRAN, and there is a notable difference. Here the multicorrelation coefficients when using BH or LWP are nearly identical (0.992 and 0.991, respectively), indicating that either is a reasonable choice for the cloud input parameter, and there is a logical explanation. In performing the sensitivity studies with MODTRAN, BH and LWP were uncorrelated since they were independently varied. But the sensitivity studies with CRM were constrained by (1) such that ln (LWP) and BH are linearly correlated with $R = 0.75$. A physical justification for (1), based upon thermodynamic arguments, is provided by *Hack* [1998]. Because of this correlation as imposed by (1), LWP, at least partially, serves as a surrogate for BH. To put it another way, although LWP might not be a direct cloud input parameter, as discussed with reference to Figure 2 for MODTRAN, for CRM it is serving as an indirect input for BH, and this has interesting implications as we next discuss.

A more pertinent set of sensitivity studies, with reference to the real atmosphere, concerns broken clouds. For this purpose we have repeated the prior overcast calculations but with randomly generated cloud amounts rather than cloud amounts of unity. In these cases, the grid-averaged LWP was determined by multiplying the cloud water density for each cloud layer by

that layer's cloud amount before integrating over the vertical column. However, there is no similar way to define a grid-averaged cloud base height, because cloud base height is not defined for the clear portion of the grid. Because of this ambiguity we have chosen the cloud base height for the overcast portion of the grid to represent that of the entire grid. These results are summarized in Figure 4 in which LWP constitutes the better cloud input parameter ($R = 0.993$) than does BH ($R = 0.987$). The suggestion, at least within the confines of the model study, is that LWP is a more realistic, although indirect, measure of cloud base height than is BH, since the latter lacks a logical grid-averaged definition. This is an interesting issue, since in section 3 we arrive at a similar result using observational data.

3. Surface Longwave Algorithm From Observational Data

In this section we test the relationships derived from the model sensitivity studies, using independent observational data which we first describe.

3.1. Data

The observational data used in this study are from the Atmospheric Radiation Measurement (ARM) Program [*Stokes and Schwartz*, 1994] at the U.S. Southern Great Plains (SGP) and the Tropical Western Pacific (TWP) sites. One of the primary objectives of ARM is to develop and test parameterizations of atmospheric water vapor, clouds, and the surface characteristics affecting atmospheric radiation. The central facility of each ARM site is designed to serve this purpose by providing high spectral resolution radiometric measurements and a detailed characterization of the atmospheric column above the facilities. The measurements include surface radiometric fluxes, clouds, aerosols, balloon-borne radiosonde profiles, regular surface meteorological parameters, and satellite observations. The SGP site is characterized with high geographical homogeneity and a variety of cloud types. The data used in this study are taken from 15 IOPs (Intensive Operation Periods) from 1994 to 1998 (Table 2) at the central facility, which is located at 36.61°N and 97.49°W in Oklahoma. The reason to use these IOP data is that GOES TOA fluxes and cloud products [*Minnis et al*., 1995] are only available for these periods at the time this work was conducted. The 15 IOPs span several years and cover different seasons (see Table 2).

Most of the surface radiometric instruments take temporally continuous measurements, while the balloon-borne soundings are launched every 3 hours, and most of the satellite measurements are taken every half hour. For the July and October 1994 IOPs, only hourly TOA measurements are available. The TOA fluxes are averaged over a 0.3° × 0.3° grid box, and the surface

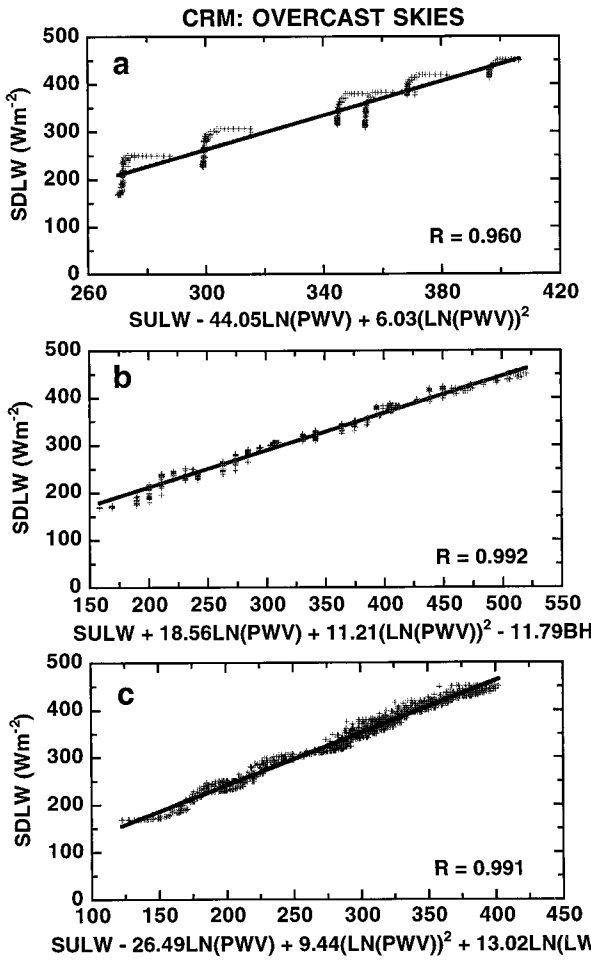

Figure 3. Same as Figure 2, but for CRM and for overcast skies.

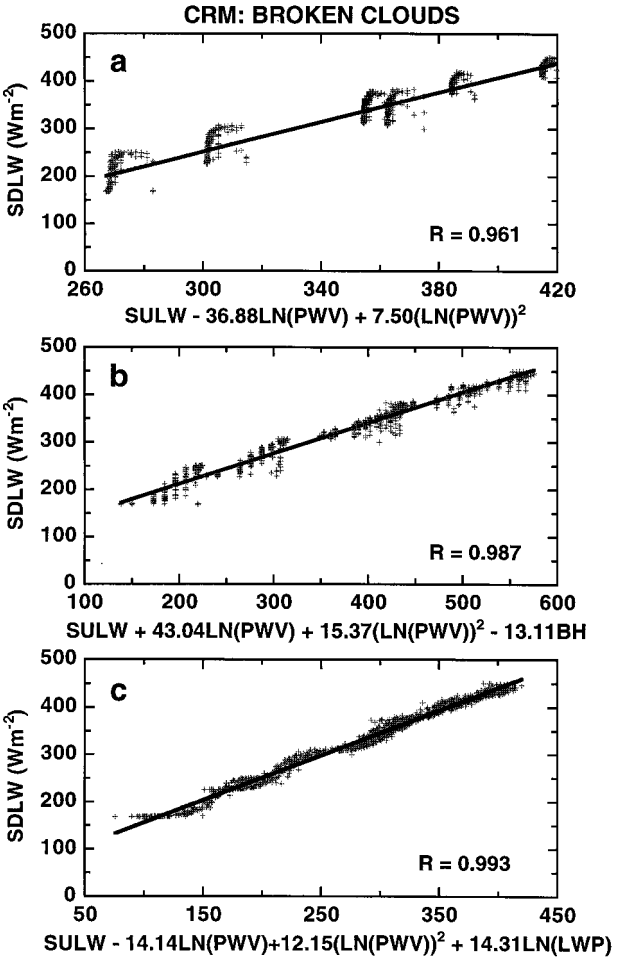

Figure 4. Same as Figure 3, but for broken clouds.

Table 2. Atmospheric Radiation Measurement Program Southern Great Plains Control Facility Intensive Operation Periods

IOP	Period	Days
April 1994	April 6–27	22
July 1994	July 11–31	21
October 1994	Oct. 23 to Nov. 15	24
July 1995	July 15 to Aug. 7	24
October 1995	Sept. 25 to Oct. 2 Oct. 8 to Nov. 1	33
April 1996	April 9 to May 9	31
March 1997	March 1–31	31
April 1997	April 1–30	30
June 1997	June 18 to July 18	30
September 1997	Sept. 15 to Oct. 5	20
December 1997	Dec. 1–31	31
January 1998	Jan. 1–31	31
February 1998	Feb. 1–28	28
April 1998	April 27 to May 17	21

fluxes are averaged into half-hourly fluxes centered at the TOA sampling time. The clear-sky identification utilizes the GOES TOA measurements [*Minnis et al*., 1995]. Cloud base heights, for the six IOPs utilized in section 3.2, have been determined from surface ceilometer measurements by M. Miller of Brookhaven National Laboratory.

The SDLW fluxes are taken from shaded and ventilated pyrgeometer measurements from the Solar and Infrared Observation Station (SIROS) or the Baseline Surface Radiation Network station (in case SIROS measurements were missing). Although the pyranometer measurements of shortwave radiation at the ARM SGP site exhibit considerable inconsistencies [e.g., *Cess et al*., 2000], it is important to emphasize that the pyrgeometer measurements of SDLW do not suffer similar shortcomings. For example, as demonstrated by *Han and Ellingson* [2000], the pyrgeometer measurements were in good agreement with observations from the adjacent atmospheric emitted radiance interferometer (AERI). There were only small steady biases between them, with the pyrgeometer measuring 1 to 4 W m^{-2} less than the AERI-based fluxes. Moreover, the relative uncertainty is estimated to be 1% by comparing two nearby pyrgeometers (K. Rutledge, personal communication, 2000). The SULW was calculated from the Surface Meteorological Observation Station (SMOS) 2-m surface air temperatures using the Stefan-Boltzmann law, since there are no consistent pyrgeometer measurements throughout all the IOPs. The SULW calculated from the SMOS air temperature is slightly lower (10 W m^{-2}) at daytime and slightly higher (8 W m^{-2}) at nighttime than the direct downward facing pyrgeometer measurement because of the diurnal variation of the near-surface air temperature as opposed to the surface skin temperature.

The microwave radiometer (MWR) measured both PWV and LWP along line of sight (LOS), which we employ in section 3.2. The PWV has been compared with the integrated total water vapor from humidity soundings for the April 1994 IOP and the October 1995 IOP as shown in Figure 5. For these two IOPs the MWR measurements underestimate PWV by 5.0%, on average, but with a considerable range in distribution (Figure 5b). The MWR underestimates PWV most of the time, but occasionally it produces a much higher value than the radiosonde measurements, which may be caused by rain or dew deposition on the sensor as we later discuss. On the other hand, radiosonde profiles, which are used as the "truth," could also be biased. For example, it has been reported that the instrument can exhibit anomalous behavior upon passing from a cloud into clear air [*Schmidlin*, 1988]. Either way, the results summarized in Figure 5 suggest a degree of uncertainty associated with the measurement of PWV.

Data representing the ARM TWP site are taken from the Manus Central Facility at the Momote Airport (2.060°S, 147.425°E). Manus is a small island located within the heart of the Pacific warm pool. The data selected for this study are for the following months: January, February, July, August, September, and October of 1997, when each parameter required for the algorithm was available. The SULW is again calculated from half-hourly averaged surface temperatures. SDLW is measured by a sky radiation sensor, while PWV and LWP are determined from LOS microwave radiometer measurements.

3.2. Data for Six SGP IOPs

We start by using data for six IOPs at the SGP site: April, July, and October from 1994 to 1996 (see Table 2). Figure 6 summarizes regression plots for the clear-sky data, with the clear-sky identification provided by GOES, in the same man-

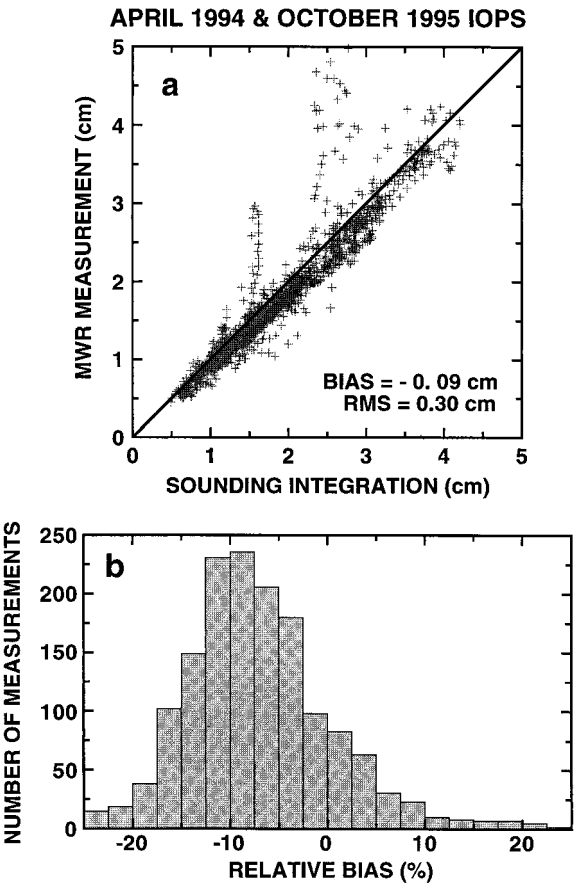

Figure 5. (a) Scatterplot of column precipitable water vapor (PWV) measured by the microwave radiometer (MWR) versus PWV determined from the sounding integration for the April 1994 and October 1995 Intensive Operation Periods (IOPs). (b) Frequency distribution of the relative bias between the column precipitable water vapor (PWV) measured by the microwave radiometer (MWR) versus PWV determined from the sounding integration.

ner as in Figure 1 for the CRM simulations, and the data provide the same conclusions as were obtained from CRM; the multivariable regression (Figure 6c) produces an excellent correlation of the data with $R = 0.978$. Likewise, Figure 7 summarizes the cloudy-sky data in a similar manner as in Figure 2 for MODTRAN and Figures 3 and 4 for CRM, and with the standard deviation included as well as R. An exception here is the last term appearing in the x axis variable of Figure 7c which, as will be discussed, was chosen since it is zero for LWP = 0. Note that inclusion of BH as a cloud input parameter (Figure 7b versus 7a) provides no enhancement in the correlation. We previously discussed difficulties in defining an average BH with respect to the CRM sensitivity studies, and such difficulties are far more pronounced when dealing with observations. The radiation fluxes, precipitable water vapor, and cloud liquid water are all half-hourly averages. An averaged cloud base height over a half-hour period, however, is not something straightforward when dealing with broken clouds (M. Miller, personal communication, 1998). The cloud base heights provided by Miller are ceilometer measurements averaged over a half-hour period and averaged together with cloud fraction (to account for cloud occurrence) and standard deviation of the cloud base (to account for horizontal inhomogeneity). Without using cloud fraction the cloud base height is certainly not representative of a half-hourly cloud status. Thus, considering the ambiguity associated with defining a temporal and spatial mean cloud base height, it is perhaps not surprising that the inclusion of BH provides no improvement in the correlation (Figure 7b versus Figure 7a). In contrast, the inclusion of LWP provides a modest improvement (Figure 7c versus 7a) which, in some circumstances, can prove to be significant as we later demonstrate. Presumably, as with the CRM sensitivity studies, this improvement is because LWP serves as a surrogate for BH, at least in an average context.

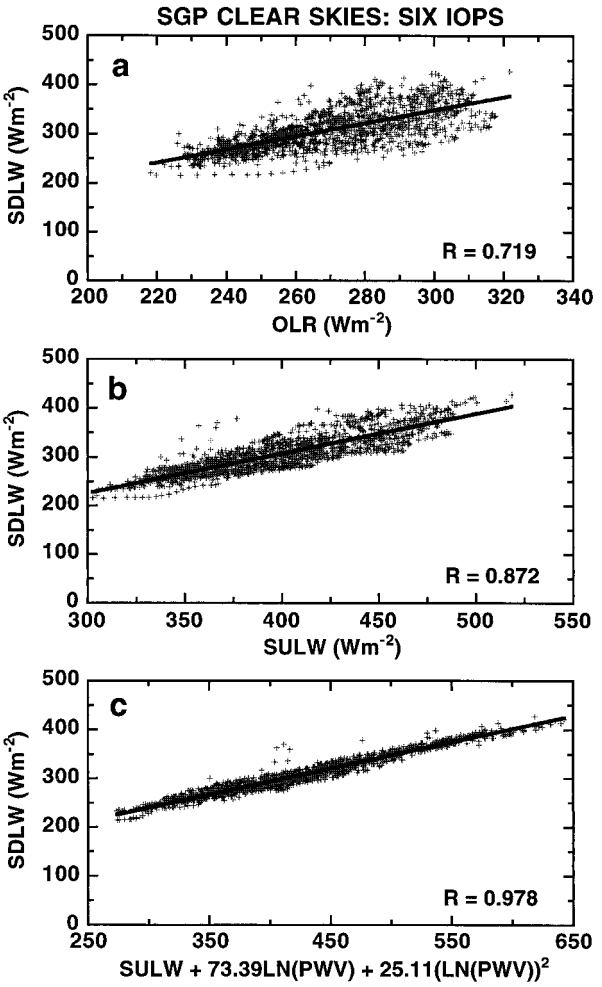

Figure 6. Same as Figure 1, but for the Southern Great Plains measurements for the first six IOPs. (See Table 2.)

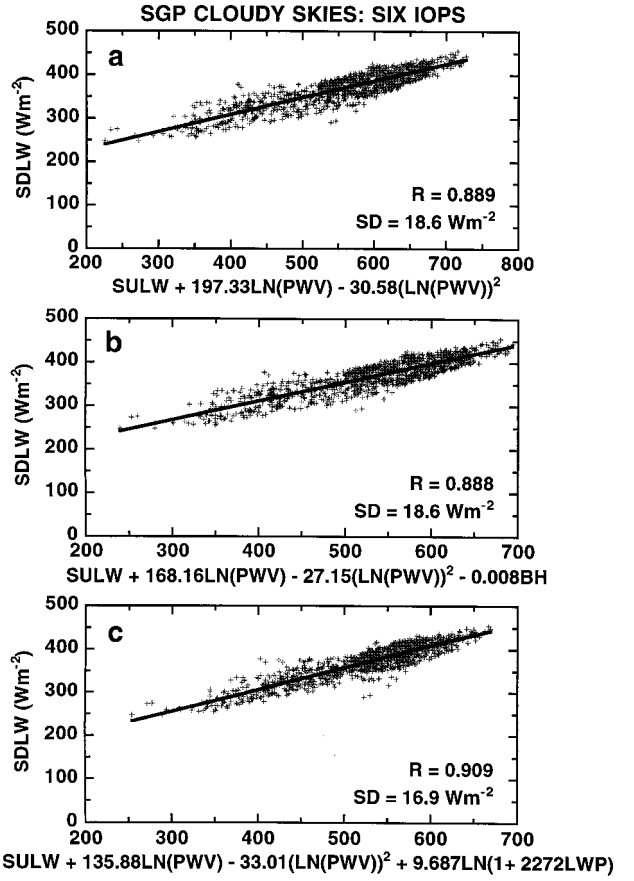

Figure 7. Same as Figure 2, but for the Southern Great Plains measurements for the first six IOPs. (See Table 2.)

The model sensitivity tests and the observational data have both shown that the clear-sky SDLW can be derived from surface temperature (i.e., SULW) and PWV. For the cloudy sky, the inclusion of LWP further increases the accuracy of the correlation. The algorithm determined from the all-sky data for the six IOPs, combining both clear (Figure 6) and cloudy (Figure 7) data, is

$$\mathrm{SDLW} = a + b\mathrm{SULW} + c\ln(\mathrm{PWV}) + d[\ln(\mathrm{PWV})]^2 + e\ln(1 + f\mathrm{LWP}), \quad (2)$$

where a, b, c, d, e, f are regression coefficients with values of 123.86, 0.444, 56.16, −3.65, 5.30, and 1226.0, respectively, and the units of PWV and LWP are in centimeters. Since LWP = 0 for clear skies, the functional form of this algorithm is such that it could be applicable to clear skies as well. Figure 8 shows scatterplots of the derived and observed SDLW for the all-sky and clear-sky data from the six IOPs. There is no bias error in

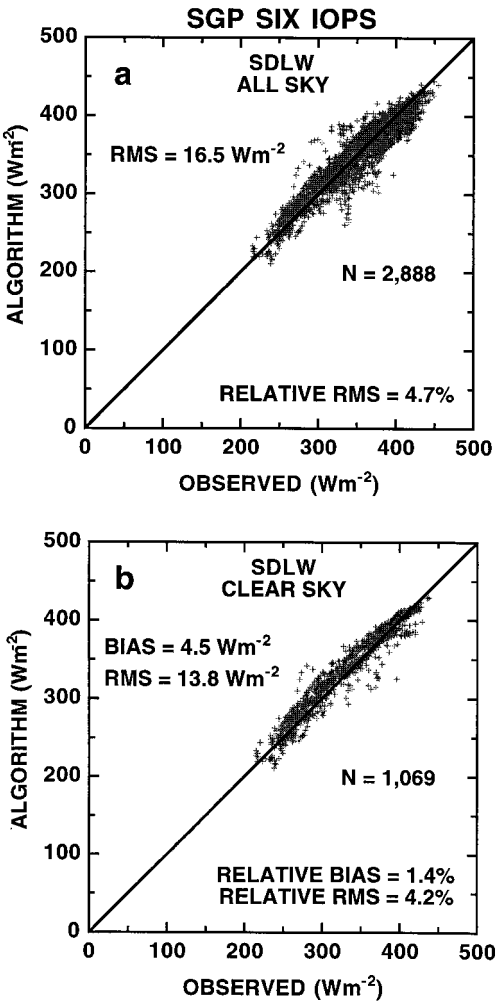

Figure 8. (a) Scatterplot of the algorithm-determined SDLW versus the measured SDLW for the Southern Great Plains all-sky measurements and for the first six IOPs. (See Table 2). *N* denotes the number of measurements. (b) Same as Figure 8a, but for clear skies.

Figure 8a (all sky), since the algorithm was determined from a regression fit to that data. But when the algorithm is applied the clear-sky subset of the data (Figure 8b), the relative bias error is only 1.4%, suggesting that a single algorithm might indeed be applicable for both all-sky and clear-sky conditions. It is interesting to note that the relative RMS errors are similar for both all-sky and clear-sky data, suggesting that the presence of clouds does not significantly increase the RMS. Although not shown in Figure 8, when restriction is made to data for which clouds are present (i.e., the data shown in Figure 7 for which clear skies are excluded), the relative bias and RMS errors are −0.7% and 4.9%, respectively. Random errors in PWV, as suggested in Figure 5, could, of course, contribute to the RMS for both all-sky and clear-sky conditions, but there is no way of quantifying their contribution to the RMS values shown in Figure 8. In sections 3.3 and 3.4 we examine the applicability of the algorithm to other data sets.

3.3. Data for the Other Nine SGP IOPs

There are nine additional IOPs from 1996 to 1998 for the SGP site which contain three winter months (Table 2), in contrast to the six original IOPs that contained no winter months. Figure 9 shows scatterplots of the derived versus observed SDLW fluxes for these nine IOPs. The bias error for the all-sky data (Figure 9a) is <1 W m^{-2}, while for the clear-sky data (Figure 9b) it is similar to that for the six original IOPs (Figure 8b). The RMS errors for both the all-sky data and clear-sky data, however, are greater in Figure 9 than in Figure 8, with some obvious positive and negative outliers in Figure 9. Although not shown in Figure 9, when restriction is made to data for which clouds are present (clear skies excluded), the relative bias and RMS errors are −0.9% and 6.1%, respectively.

The positive outliers in Figure 9a correspond mainly to the large values of PWV shown in the PWV versus SULW scatterplot of Figure 10b; note that similar outliers are largely absent in the data for the original six IOPs (Figure 10a). According to the ARM instrument mentor (J. Liljegren, personal communication, 1997), precipitable water larger than 5 cm is very rare in Oklahoma, and if the cloud liquid water is >0.1 cm, then it is most likely raining or wet with other forms of precipitation. From the LWP versus PWV scatterplot of Figure 10d, the large PWV data likewise correspond to LWP normally >0.2, and these excursions are also largely absent for the original six IOPs (Figure 10c). Moisture detectors were in-

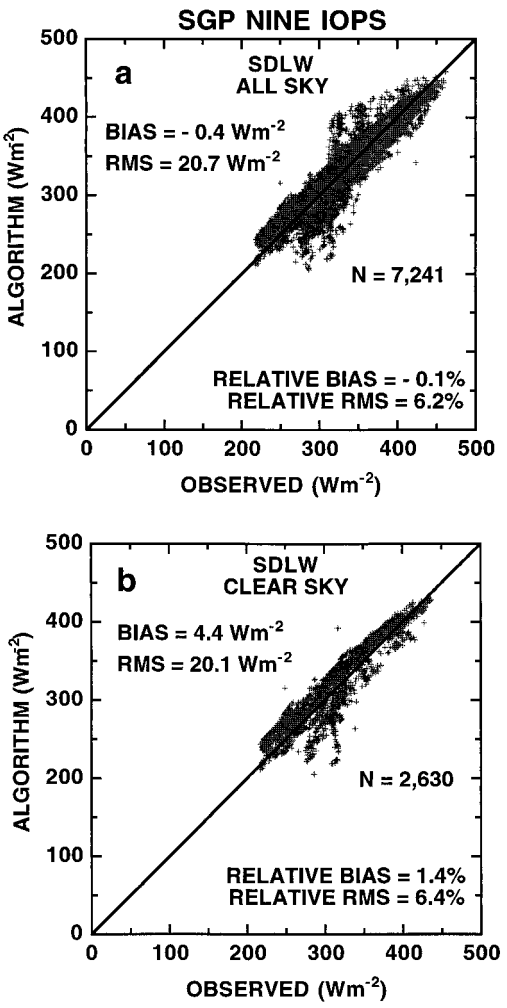

Figure 9. Same as Figure 8, but for the latter nine IOPs. (See Table 2.)

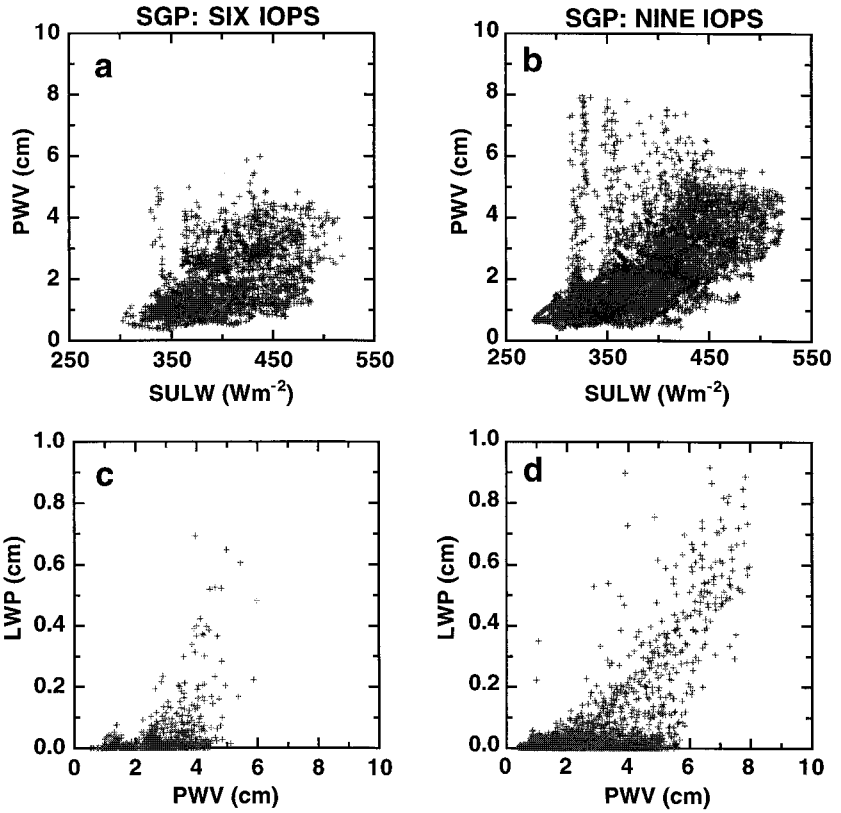

Figure 10. Scatterplot of PWV versus SULW for the first six IOPs at the Southern Great Plains. (b) Same as Figure 10a, but for the latter nine IOPs. (c) Scatterplot of LWP versus PWV for the first six IOPs. (d) Same as Figure 10c, but for the latter nine IOPs.

stalled on the MWRs in 1993 so as to flag data as "wet" if there was moisture on the MWR window. And when moisture was detected, a heater was turned on to dry the window. However, sometimes the detector dries before the window, and that might explain the positive outliers in Figure 10b and in turn in Figure 9a.

Data for the negative outliers in Figure 9a are located in the lower left corners of Figures 10b and 10d, which means that the weather for these cases was extremely cold and dry. The average precipitable water and cloud liquid water for negative biases exceeding 50 W m^{-2} in Figure 9a was 0.64 cm and 0.0055 cm (0.003 cm of cloud liquid water is considered clear), respectively. However, the average surface relative humidity was always >92%. From the weather log we found well-developed overcast stratus fractus over the central facility on January 9, 1998, but the MWR instrument recorded essentially zero LWP on that day, and a data inconsistency of this type would result in the algorithm producing a negative bias. This would not, however, explain the negative biases for clear skies shown in Figure 9b, although their population is considerably less than in Figure 9a.

The data anomalies discussed above are primarily restricted to the three winter months (December 1997, January 1998, and February 1998) and correspondingly produce excessive RMS errors as demonstrated in Figure 11. For the other months the algorithm's bias and RMS errors are quite small. When the three winter months are deleted, the average RMS errors for the remaining six IOPs become comparable to those for the original six IOPs (Figure 8): RMS = 15.9 W m^{-2} for all skies and RMS = 15.0 W m^{-2} for clear skies.

3.4. Data for the TWP Manus Site

The tropical Pacific warm pool is characterized by high surface temperatures, an extremely humid lower atmosphere, and extended cirrus clouds caused by deep convection. The SDLW does not have variations as large because of minimal variations of surface temperature and the abundant moisture in the lower atmosphere. The high cirrus clouds, predominantely composed of ice and thus not contributing to the measured LWP, hardly affect the surface downwelling longwave flux. The standard deviations of SULW and SDLW for the 6 months of Manus data are only 10 and 15 W m^{-2}, respectively, and the average PWV is 5.1 cm, much greater than for the Oklahoma site.

Figure 12 shows scatterplots of the derived SDLW versus the observed SDLW, with the derived SDLW evaluated from the algorithm based on the data for the six SGP IOPs. Since TOA clear-sky identification is not available for this data set, the LWP was used as the clear-sky criterion; a sample was regarded as clear when LWP was <0.003 cm. Although not shown in Figure 12, when restriction is made to data for which clouds are present (clear skies excluded), the bias and RMS errors are 7.0 W m^{-2} and 10.8 W m^{-2}, respectively. The algorithm derived from the data for the six SGP IOPs is thus very successful in replicating the observed SDLW, producing minimal bias and RMS errors. Because of the considerable differences in atmospheric state between Oklahoma and the

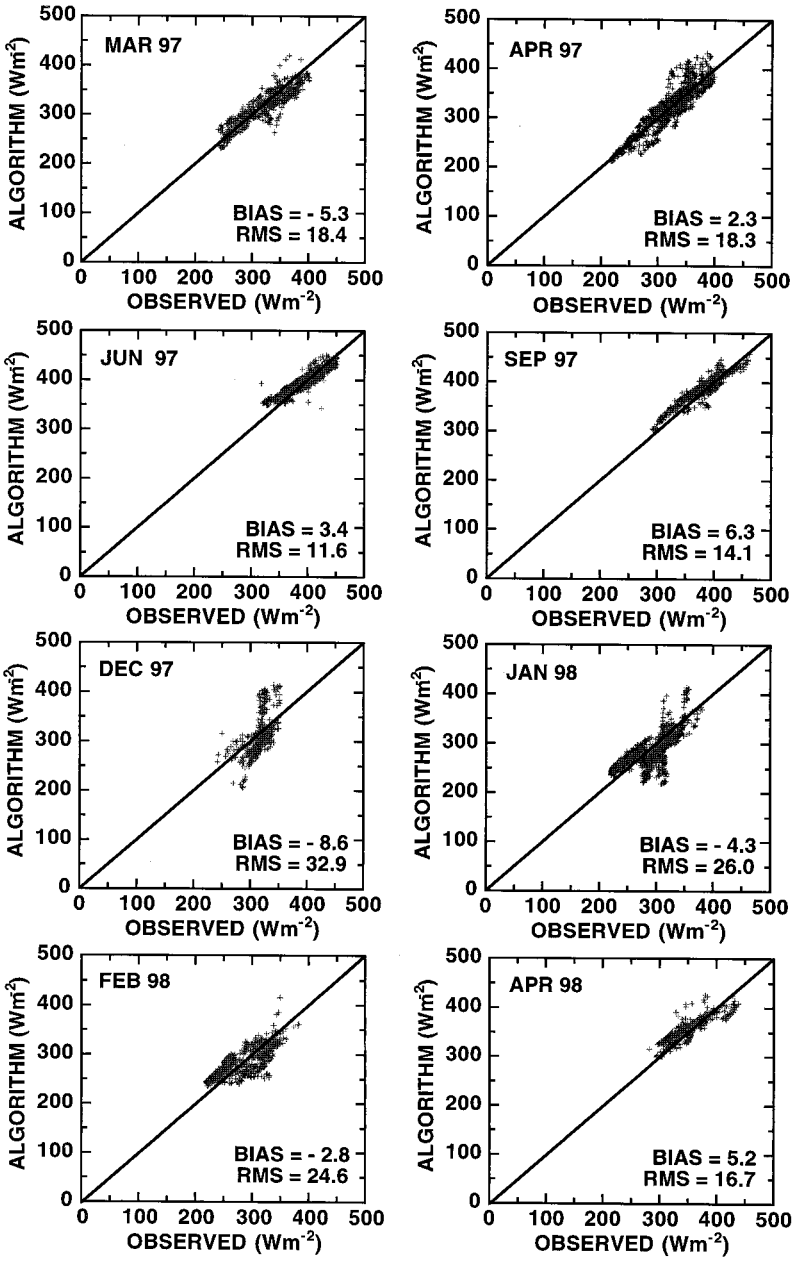

Figure 11. Scatterplots of the algorithm-determined SDLW versus that measured at the Southern Great Plains for each of the latter eight IOPs. (See Table 2.)

tropical western Pacific, this suggests that the Oklahoma-derived algorithm may have broad geographic applicability. The results shown in Figure 12 further underscore the point that a single algorithm appears to be applicable for both clear and cloudy conditions.

The TWP data also serve to demonstrate the importance of including the last term in (2), despite the fact that comparing Figure 7c versus 7a for the SGP data indicates only a modest improvement in the correlation due to this term. The "no LWP term" bias and RMS errors shown in Figure 12 correspond to using the algorithm, as given by (2), with the last term deleted and reevaluating the regression coefficients a, b, c, and d, again using the six SGP IOPs. Figure 12a shows that including LWP provides a modest improvement in both the bias and RMS errors, as is consistent with the modest improvement in correlation for Figure 7c relative to 7a. But for clear skies, as demonstrated in Figure 12b, the improvement is substantial. This is because the "no LWP term" algorithm applies to an average LWP (in this case for the six SGP IOPs), whereas for clear skies (2) is being applied to the limit LWP = 0. Thus the inclusion of the last term in (2) is important if an algorithm derived from all-sky data is to be applied to clear-sky conditions.

4. Summary and Discussion

The model sensitivity tests demonstrate that for clear skies the SULW and the column PWV mainly determine the surface downwelling longwave flux. For the cloudy skies, however, the situation becomes more complex. Logic would dictate that cloud base height should significantly impact SDLW, since it

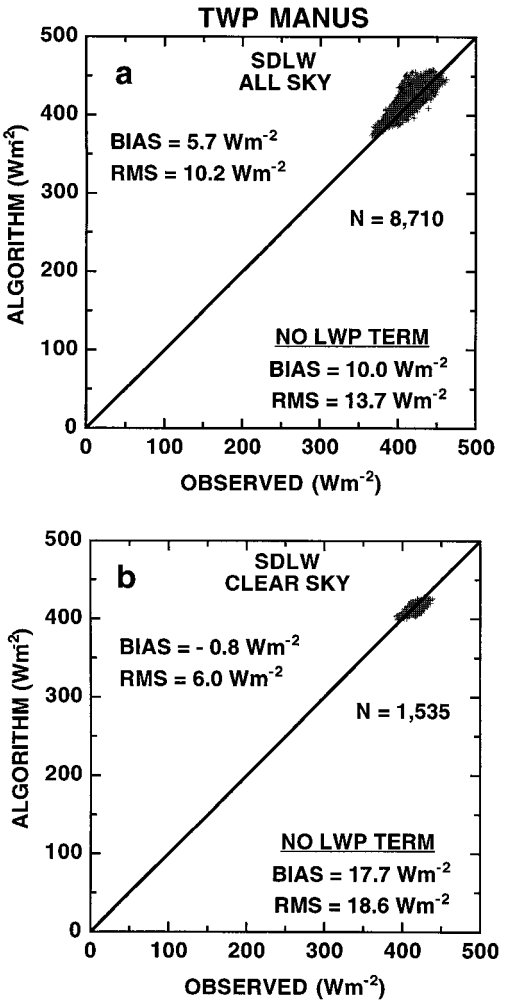

Figure 12. Same as Figure 8, but for the 6 months of measurements made at Manus Island in the tropical western Pacific (TWP).

determines the emission temperature of the cloud bottom, whereas cloud LWP should have little impact because the cloud base emissivities are unity for clouds that impact SDLW. For overcast conditions the sensitivity studies with MODTRAN are consistent with this expectation, but for CRM, cloud base altitude and LWP are found to be equally valid cloud input parameters. This is because CRM contains the parameterization in CCM3 that relates LWP to cloud altitude, a parameterization based on thermodynamic arguments [*Hack*, 1998], such that LWP serves as a surrogate for cloud base altitude. This has interesting implications concerning the broken-cloud simulations with CRM for which LWP is found to be a better cloud parameter for determining SDLW than is cloud base height, since the latter lacks a logical average definition when applied to a grid containing both clear and overcast regions.

The observational data from the ARM SGP central facility and the TWP Manus central facility have shown similar relations as obtained from the model sensitivity studies. A suggestive algorithm relating SDLW to SULW, PWV, and LWP, based upon a multiple regression of all-sky SGP data, indicates that a single algorithm might be applicable to both cloudy and clear conditions as well as being geographically invariant, since the SGP-derived algorithm produces SDLW results that agree extremely well with measured SDLW values at the TWP site. We emphasize, however, that the present study is aimed at developing strategies for algorithm development, rather than developing an algorithm per se. Only two geographical regions have been considered in this study, and we have less confidence on how this algorithm will work in extremely cold and dry areas for which the SDLW is more sensitive to clouds, since there is little water vapor in the atmosphere, and most of the clouds are in the form of ice particles. Ice clouds have little impact for the SGP and TWP regions studied here, since they are too high in the atmosphere to impact SDLW. Also, as pointed out with reference to Figures 5 and 10, there are possible uncertainties with respect to the microwave radiometer measurements at the SGP site, and it is our understanding that eventually this data will be reprocessed.

No direct comparisons have been made between the current suggestive algorithm and previous algorithms. The empirical formulae are known to be unable to adequately reproduce clear-sky fluxes [*Breon et al*., 1991] and are even worse for cloudy-sky fluxes [*Fung et al*., 1984]. Most of the satellite methods are highly dependent on cloud input parameters, with typical RMS errors of 6–8% [*Frouin et al*., 1988]. The current suggestive algorithm is simple and quite accurate, with only 2–5% RMS errors when applied to the SGP and TWP data.

Acknowledgments. We are grateful to the following individuals for their advice and assistance: Marvin Geller, Minghua Zhang, and Duane Waliser of SUNY Stony Brook; Patrick Minnis, Thomas Charlock, and Tim Alberta of NASA Langley Research Center; Mark Miller and Joyce Tichler of Brookhaven National Laboratory; James Lilegren and Marvin Wesley of the ARM Data Center; and Ruchong Yu of the Institute of Atmospheric Physics, Chinese Academy of Sciences. This work was supported by the DOE ARM Program through grant DEFG0290ER61063, by DOE grant DEFG0285ER60314, and by the CERES project through NASA contract NAS1-981421, all to SUNY Stony Brook.

References

Abreu, L. W., and G. P. Anderson, The MODTRAN 2/3 report and LOWTRAN 7 model, Ontar Corp., Air Force Phillips Lab./ Geophys. Dir., Hascom Air Force Base, Mass., 1996.

Acharya, P. K., S. M. Adler-Golden, G. P. Anderson, A. Berk, L. S. Bernstein, J. H. Chetwynd, and M. W. Matthew, MODTRAN version 3.7/4.0 users' manual, Air Force Res. Lab., Space Vehicles Dir., Hanscom Air Force Base, Mass., 1998.

Berliand, M. E., and T. G. Berliand, Determining the net long-wave radiation of the Earth with consideration of the effect of cloudiness, *Isv. Akad. Nauk SSSR*, *Ser. Geofis*., *1*, 1952.

Breon, F.-M., R. Frouin, and C. Gautier, Downwelling longwave irradiance at the ocean surface: An assessment of in situ measurements and parameterizations, *J. Appl. Meteorol*., *30*, 17–31, 1991.

Brutsaert, W., On a derivable formula for long-wave radiation from clear skies, *Water Resour. Res*., *11*, 742–744, 1975.

Cess, R. D., T. Qian, and M. Sun, Consistency tests applied to the measurements of total, direct, and diffuse shortwave radiation at the surface, *J. Geophys. Res*., *105*, 24,881–24,887, 2000.

Frouin, R., C. Gautier, and J. J. Morcrette, Downward longwave irradiance at the ocean surface from satellite data: Methodology and in-situ validation, *J. Geophys. Res*., *93*, 597–619, 1988.

Fung, I., D. E. Harrison, and A. A. Lacis, On the variability of the net longwave radiation at the ocean surface, *J. Geophys. Res*., *89*, 177–193, 1984.

Gupta, S. K., A parameterization for longwave surface radiation from sun-synchronous satellite data, *J. Clim*., *2*, 305–320, 1989.

Gupta, S. K., W. L. Darnell, and A. C. Wilber, A parameterization for longwave surface radiation from satellite data: Recent improvements, *J. Applied Meteorol*., *31*, 1361–1367, 1992.

Hack, J. J., Sensitivity of the simulated climate to a diagnostic formulation for cloud liquid water, *J. Clim*., *11*, 1497–1515, 1998.

Han, D., and R. G. Ellingson, An experimental technique for testing the validity of cumulus cloud parameterizations for longwave radiation calculations, *J. Appl. Meteorol*., *39*, 1147–1159, 2000.

Harshvardhan, D. A. Randall, and D. A. Dazlich, Relationship between the longwave cloud radiative forcing at the surface and the top of the atmosphere, *J. Clim*., *3*, 1435–1443, 1990.

Idso, S. B., A set of equation for full spectrum and 8- to 14-μm and 10.5- to 12.5-μm thermal radiation from cloudless skies, *Water Resour. Res*., *17*, 295–304, 1981.

Idso, S. B., and R. D. Jackson, Thermal radiation from the atmosphere, *J. Geophys. Res*., *74*, 5397–5403, 1969.

Inamdar, A. K., and V. Ramanathan, Physics of greenhouse effect and convection in warm oceans, *J. Clim*., *7*, 715–731, 1994.

Inamdar, A. K., and V. Ramanathan, Clouds and the Earth's Radiant Energy System (CERES) Algorithm Theoretical Basis Document: Estimation of longwave surface radiation budget from CERES (subsystem 4.6.2), NASA, Washington, D. C., June 2, 1997.

Kiehl, J. T., Modeling and validation of clouds and radiation in the NCAR Community Climate Model, in *Proceedings of the ECMWF/WCRP Workshop on Clouds, Radiative Transfer and the Hydrological Cycle*, *Reading, England, UK*, November 12–15, 1990, pp. 41–450, Eur. Cent. for Medium-Range Forecasts, Reading, England, UK, 1991.

Kiehl, J. T., J. J. Hack, G. B. Bonan, B. A. Boville, B. P. Briegleb, D. L. Williamson, and P. J. Rasch, Description of the NCAR Community Climate Model (CCM3), *NCAR Tech. Note*, *NCAR/TN-420+STR*, 1996.

Kneizys, F. X., E. P. Shettle, L. W. Abreu, J. H. Chetwynd, G. P. Anderson, W. O. Gallery, J. E. Selby, and S. A. Clough, Users Guide to LOWTRAN 7, *Tech. Rep. AFGL-TR-88-0177*, U.S. Air Force Geophys. Lab., Hanscom Air Force Base, Mass., 1988.

Manabe, S., and R. T. Wetherald, Thermal equilibrium of the atmosphere with a given distribution of relative humidity, *J. Atmos. Sci*., *24*, 241–259, 1967.

Minnis, P., W. L. Smith Jr., D. P. Garber, J. K. Ayers, and D. R. Doelling, Cloud properties derived from GOES-7 for spring 1994 ARM intensive period using version 1.0.0 of ARM Satellite Data Analysis Program, *NASA Ref. Publ. 1366*, 1995.

Prata, A. J., A new long-wave formula for estimating downward clear-sky radiation at the surface, *Q. J. R. Meteorol. Soc*., *122*, 1127–1151, 1996.

Ramanathan, V., Scientific use of surface radiation budget data for climate studies, surface radiation budget for climate application, in *Surface Radiation Budget for Climate Applications*, edited by J. T. Suttles and G. Ohring, *NASA Ref. Publ. 1169*, 57–86, 1986.

Ramanathan, V., and P. Downey, A nonisothermal emissivity and absorptivity formulation for water vapor, *J. Geophys. Res*., *91*, 8649–8666, 1986.

Rothman, L. S., et al., The HITRAN molecular database: Edition of 1991 and 1992, *J. Quant. Spectrosc. Radiat. Transfer*, *48*, 469–507, 1992.

Satterlund, D. R., An improved equation for estimating long-wave radiation from the atmosphere, *Water Resour. Res*., *15*, 1649–1650, 1979.

Schmetz, P., J. Schemtz, and E. Raschke, Estimation of daytime downward longwave radiation at the surface from satellite and grid point data, *Theor. Appl. Climatol*., *37*, 136–149, 1986.

Schmidlin, F. J., WMO international radiosonde comparison, phase II, Instruments and observing methods report, *WMO/TD-312*, *29*, World Meteorol. Org., Geneva, 1988.

Smith, W. L., and H. M. Woolf, Geostationary satellite sounder (VAS) observations of longwave radiation flux, *WMO World Clim. Progr. Doc. WCP-70*, 36 pp., World Meteorol. Org., Geneva, 1983.

Stephens, G. L., A. Slingo, M. J. Webb, P. J. Minnet, P. H. Daun, L. Kleinman, I. Wittmeyer, and D. A. Randall, Observations of the Earth's Radiation Budget in relation to atmospheric hydrology, 4, Atmospheric column radiative cooling over the world's oceans, *J. Geophys. Res*., *99*, 18,585–18,604, 1994.

Stokes, G. M., and S. Schwartz, The atmospheric radiation measurement (ARM) program: Programmatic background and design of the cloud and radiation test bed, *Bull. Am. Meteorol. Soc*., *75*, 1201–1221, 1994.

Sun, D. Z., and A. H. Oort, Humidity-temperature relationships in the tropical troposphere, *J. Clim*., *8*, 1974–1987, 1995.

Swinbank, W. C., Longwave radiation from clear skies, *Q. J. R. Meteorol. Soc*., *89*, 339–348, 1963.

R. D. Cess, Marine Sciences Research Center, State University of New York, Stony Brook, NY 11794-5000. (rcess@notes.cc.sunysb.edu)

Y. Zhou, Analysis Branch, Climate Prediction Center, NOAA/NWS/NCEP, Washington, DC 20233. (yzhou@ncep.noaa.gov)

(Received September 29, 2000; revised February 5, 2001;
accepted February 15, 2001.)